NUCLEOSYNTHESIS AND METEORITES

For a splendid introduction, please see
Cosmochemistry
H Y McSween, Jr. and G R Huss (on reserve in Peridier)

1. Contributions to the Standard Abundance Table/Curve:
   See earlier discussion, especially request to read
   Lodder, Palme & Gail (2009) review of CI1 carbonaceous
   meteorites, solar photospheric abundances etc.

2. Radioisotopes as chronometers (Cosmochemistry, Chap. 8)
   -- Long-lived radionuclides: incorporated into solar
      nebula and a fraction still alive today --> ages of
      materials and under some circumstances time since
      radionuclides synthesized (cosmochronology).
      Table 8.1 lists accessible radionuclides.
   -- Short-lived radionuclides - see Table 8.8
      See discussion shortly of 26Al-26Mg - a UT success story

3. Presolar grains (Cosmochemistry, Chap. 5)
   -- Xenon anomalies (and occluded gases)
   -- isolation and characterization of grains (Table 5.1)
   -- identification of stellar sources: AGB stars, SN, Novae and ?

4. Cosmogenic nuclides (Cosmochemistry pp.340 - 344)
   -- Nuclides produced by cosmic rays experiencing nuclear
      reactions (spallation or secondary neutron capture, principally)
      in meteorites. See Table 9.1. Estimate CR exposure ages.

Advances in laboratory instrumentation critical to new discoveries:
   -- rarer isotopes in grains and for investigations of radionuclides,
      analyses of individual grains rather than
      aggregates of grains, ...

For presolar grains: emphasis on isotopic ratios, e.g. 12C/13C vs 14N/15N
      why not study abundance anomalies?

Nittler (2003) quote

Table 8.1 Long-lived radionuclides used in cosmochemistry

Nuclide	Half-life (years)	Daughter isotope	Decay mode*
^{40}K	1.27×10^{9}	^{40}Ar (11%)	E.C.
		^{40}Ca (89%)	β^-
^{87}Rb	4.88×10^{10}	^{87}Sr	β^-
^{138}La	1.05×10^{11}	^{138}Ba (34%)	E.C.
		^{138}Ce (66%)	β^-
^{147}Sm	1.06×10^{11}	^{143}Nd	α
^{176}Lu	3.75×10^{10}	^{176}Hf	β^-
^{187}Re	4.12×10^{10}	^{187}Os	β^-
^{190}Pt	4.50×10^{11}	^{186}Os	α
^{238}U	4.47×10^{9}	^{206}Pb	α, (S.F.)
^{235}U	7.04×10^{8}	^{207}Pb	α, (S.F.)
^{232}Th	1.40×10^{10}	^{208}Pb	αt, (S.F.)

* Decay modes: E.C. = electron capture, β^- = beta decay, α = alpha decay, S.F. = spontaneous fission.

Al-26 -- Mg-26 evolution

Al-26 decays by beta+ and EC to excited Mg-26 with a half-life of 730,000 yrs. Excited Mg-26 by emitting a 1806 keV gamma ray

Stable isotope of Al is Al-27

Stable isotopes of Mg are Mg-24, 25 and 26

If live Al-26 was in solar system at its birth, it will have decayed to stable Mg-26 and produced an anomalous Mg-26 abundance which should be correlated with the sample's Al-27 abundance.

Construct a plot of x = 27Al/26Mg and y = 26Mg/24Mg
(Why 27Al/26Mg?)

Early - first? - indication that there is/was live Al-26 in the Galaxy.

Pre-solar graphite, SiC and Si3N4 grains can have high levels of Al-26
(Groopman et al. 2015, ApJ, 809, 31)

Al-26 emission from Galaxy now mapped = Nucleosynthesis in 3D!
-- See Iliadis - Color figure 12
-- See Diehl, Hartmann & Prantzos Chapter 7 in Astronomy with Radioactivities
Figure 7.8, 7.11

Table 8.8 Short-lived radionuclides used in cosmochemistry

Nuclide N_R	Half-life (years)	Daughter isotope(s)	Decay mode*	Stable nuclide N_S	$(N_R/N_S)_0$
^{7}Be	53 days	^{7}Li	E.C.	^{9}Be	
^{10}Be	1.5×10^{6}	^{10}B	β^{-}	^{9}Be	1×10^{-3}
^{14}C	5715	^{14}N	β^{-}	^{12}C	
^{22}Na	2.604	^{22}Ne	β^{+}	^{23}Na	
^{26}Al	**7.3×10^{5}**	**^{26}Mg**	**β^{+}, E.C.**	**^{27}Al**	**5×10^{-5}**
^{36}Cl	3.01×10^{5}	^{36}Ar (98.1%)	β^{-}	^{35}Cl	5×10^{-6}
		^{36}S (1.9%)	E.C., β^{+}		
^{41}Ca	1.03×10^{5}	^{41}K	E.C.	^{40}Ca	1.5×10^{-8}
^{44}Ti	59.9	^{44}Ca (via ^{44}Sc)	E.C., E.C.		
^{53}Mn	**3.7×10^{6}**	**^{53}Cr**	**E.C.**	**^{55}Mn**	**9.1×10^{-6}**
^{60}Fe	1.5×10^{6}	^{60}Ni (via ^{60}Co)	β^{-}	^{56}Fe	$(5–10) \times 10^{-7}$
^{92}Nb	36×10^{6}	^{92}Zr	E.C.		
^{107}Pd	6.5×10^{6}	^{107}Ag	β^{-}	^{108}Pd	2×10^{-5}
^{129}I	**1.7×10^{7}**	**^{129}Xe**	**β^{-}**	**^{127}I**	**1×10^{-4}**
^{146}Sm	**1.03×10^{8}**	**^{142}Nd**	**α**	**^{144}Sm**	**8×10^{-3}**
^{182}Hf	**8.9×10^{6}**	**^{182}W**	**β^{-}**	**^{180}Hf**	**$\tilde{9}7 \times 10^{-5}$**
^{244}Pu	8.2×10^{7}	^{208}Pb, Xe isotopes	α, S.F.	^{232}Th	3×10^{-3}

* E.C. = electron capture, β^{-} = beta decay, β^{+} = positron decay, α = alpha decay, S.F. = spontaneous fission.

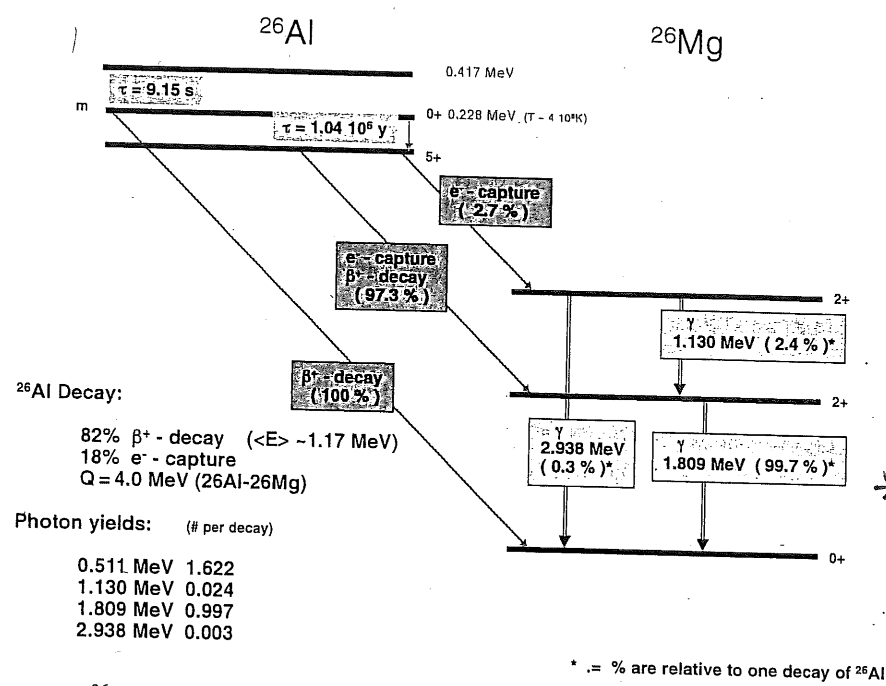

Fig. 1.3 ^{26}Al decay. The ^{26}Al nucleus ground state has a long radioactive lifetime, due to the large spin difference of its state to lower-lying states of the daughter nucleus ^{26}Mg. An isomeric excited state of ^{26}Al exists at 228 keV excitation energy. If thermally excited, ^{26}Al may decay through this state. Secondary products, lifetime, and radioactive energy available for deposits and observation depend on the environment

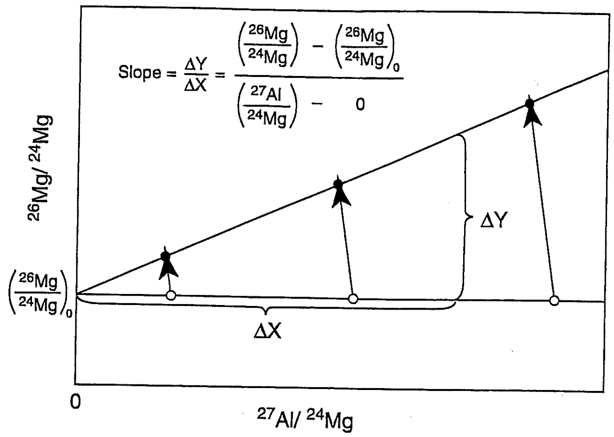

Schematic drawing of an ^{26}Al–^{26}Mg evolution diagram (isochron diagram). The slope of such a diagram gives the $(^{26}Al/^{27}Al)_0$ ratio and the intercept gives the $(^{26}Mg/^{24}Mg)_0$ ratio for the system.

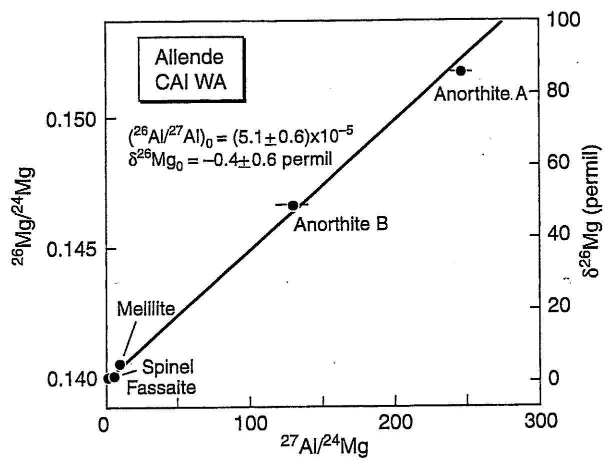

^{26}Al–^{26}Mg evolution diagram of CAI WA from Allende, the first sample to show clear evidence of live ^{26}Al in the solar system. $^{26}Mg/^{24}Mg$ ratios are given on the left vertical axis and delta values calculated relative to terrestrial magnesium are given on the right. After Lee *et al.* (1977).

$$Slope = \frac{\Delta Y}{\Delta X} = \frac{\left(\frac{^{26}Mg}{^{24}Mg}\right)_{meas} - \left(\frac{^{26}Mg}{^{24}Mg}\right)_0}{\left(\frac{^{27}Al}{^{24}Mg}\right)_{meas} - 0}$$

The ^{24}Mg in this equation represents the indigenous magnesium in the sample and so i same in numerator and denominator and can be eliminated. The radiogenic $^{26}Mg^*$ equal measured ^{26}Mg minus the original ^{26}Mg in the sample, so the above equation become

$$Slope = \frac{^{26}Mg_{meas} - {}^{26}Mg_0}{^{27}Al_{meas}} = \frac{^{26}Mg*}{^{27}Al} = \left(\frac{^{26}Al}{^{27}Al}\right)_0 \quad (8$$

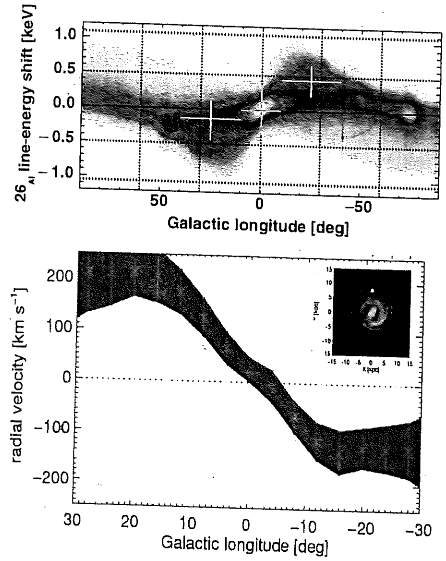

Fig. 7.11 Kinematics of ^{26}Al towards the inner Galaxy, from INTEGRAL/SPI measurements. *Top:* Indications of ^{26}Al line position variation with Galactic longitude(Diehl et al., 2006a). The underlying colors show the expected *line brightness* and velocity shift versus longitude, data points are from first 1.5 years of INTEGRAL observations. *Bottom:* Longitude-velocity diagram, for hot ISM as traced through ^{26}Al in the inner Galaxy. From 5 years of observation, the ^{26}Al signal can be determined for narrower longitude intervals (here $\delta l = 16°, \delta b = 10°$), and shows the trend from the Galaxy's large-scale rotation. (Kretschmer et al., in prep. (2010))

There is one independent signature which can tell us about distances: The Doppler shift of spectral lines will encode the relative velocity of the source region with respect to the observer. Such information is widely used in disentangling brightness information along the observer's line of sight, for example in 21 cm mapping of atomic hydrogen thoughout the Galaxy (Hartmann and Burton, 1997). With Ge spectrometry of the ^{26}Al gamma-ray line, an important step towards this direction was taken with the INTEGRAL mission (Fig. 7.11). These data show Doppler-shifts in the ^{26}Al line consistent with expectation from the Galaxy's large-scale rotation. This is evidence that a substantial part or all of the observed ^{26}Al gamma-ray brightness towards the inner Galaxy indeed originates there, rather than in specific regions more nearby. Therefore, we may regard as a rather secured first-order approximation a large-scale geometrical model of ^{26}Al source distributions within the Galaxy, such as inferred from molecular cloud material, from free electrons, or from dust thermal emission, and normalize the projection of such a spatial distribution onto the sky with the observed ^{26}Al gamma-ray line brightness to determine the total ^{26}Al mass in our Galaxy. This has been done in several studies, based on COMPTEL and on INTEGRAL data. They all find an ^{26}Al amount between 1.5 and 3 $M_\odot$, depending on data and models used. Diehl et al. (2006a) obtain $(2.8 \pm 0.8)\ M_\odot$ of ^{26}Al.

This ^{26}Al mass determinatic
Galaxy now allows a compariso
didate sources on theoretical g
massive stars $2.1 \pm 1.1\ M_\odot$ were
Rayet phase was estimated to cc
$\sim$3 uncertainty (see Prantzos &
ties are due to the incomplete ce
2001) and yield uncertainties fro
assessed a Galactic contribution
2005), accounting for new insigh
also Chap. 4). Models for these
total massive-star yields of abou
Models for novae and AGB stai
novae ranged from 0.1 to 5 $M_\odot$
progenitor knowledge, and from
model. About 0.2 $M_\odot$ of Galactic
factor $\sim$3 uncertainty (see Jose ai
osynthesis, but Chap. 5 presents
stars were once thought to be pc
Charbonnel, 1997), their contribu
of massive stars (see Chap. 3). N
as ^{26}Al producers from interstell
Nittler, 2004, for a review, and (
are copious dust producers, more
that interstellar grain samples of n
producing sources.

If we assume that massive st
their theoretical yield estimates
function to compare with the ob
such comparison is the Galactic s
7.9). ^{26}Al measurements, as inte
core-collapse supernova rate of
is consistent with other determina
trace objects in the solar vicinity a
which are assumed to be similar
a detailed comparison and discus
though limited in precision both
uncertainties, provide an alterna
for our Galaxy, which is differen
core-collapse rate among method

The global line width of the 2
large-scale rotation within the Ga
in the presumably-hot interstell
time of its decay, after its ejectio
interstellar space for $\simeq 1$ My, Co

2. Isolation and analysis of presolar grains

Hints that presolar grains might be present in meteorites surfaced in the 1960s, but it was the development of both new chemical dissolution techniques and new isotopic microanalysis techniques, especially secondary ion mass spectrometry (SIMS), that finally led to their successful isolation and identification as presolar stardust in the late 1980s. The history of this discovery has been reviewed by [2]. The known types of presolar grains are summarized in Table 1; example micrographs are shown in Fig. 1.

It is fortuitous that among the mineral phases that condense in stars are tough, acid-resistant phases like SiC and Al_2O_3, enabling their isolation from meteorites by essentially dissolving away everything else in harsh acids. This has often been likened to burning down a haystack to find a hidden needle and immediately raises the crucial issue of sampling bias. There are probably other presolar phases present in meteorites, especially silicates, which are dissolved in the procedures currently used to concentrate presolar grains. An additional bias comes from grain size: most work on individual presolar grains has been on particles at least 1 μm in diameter. In contrast, typical circumstellar and interstellar grain sizes inferred from astronomical observations are closer to 0.1 μm.

Ultimately, obtaining a representative sample of the presolar solid materials that went into forming the solar system will require new chemical and/or microanalytical techniques, many of which are under development. Two recent advances discussed here are resonance ionization mass spectrometry (RIMS), which allows measurement of ppm-level trace elements in micron-sized grains with elimination of isobaric interferences, and the new Cameca NanoSIMS 50 ion probe, which allows isotopic measurements of major and minor elements to be made on a 50–200 nm scale, compared with the 1 μm scale of previous SIMS instruments. As a dramatic example of the new frontier opened by the NanoSIMS, Messenger et al. [4] recently reported the in situ discovery of sub-micron presolar silicates in interplanetary dust particles.

Nittler 2003 Earth Planetary Science Letters 209, 259

Table 5.1 Known types of presolar grains

Name	Composition	Size	Matrix-normalized abundance
Diamond	C	1–2 nm	1500 ppm
Silicon carbide	SiC	0.1–10 μm	10–15 ppm
Graphite	C	0.1–20 μm	5–10 ppm
TiC, MoC, ZrC, RuC, FeC, Fe–Ni	Inside other materials	1–25 nm	n.d.
Spinel	$MgAl_2O_4$	0.1–20 μm	1.2 ppm
Corundum	Al_2O_3	0.2–3 μm	100 ppb
Hibonite	$CaAl_{12}O_{19}$	1–5 μm	20 ppb
TiO_2	TiO_2	n.d.	<10 ppb
Si_3N_4	Si_3N_4	1–5 μm	1–20 ppb
Forsterite	Mg_2SiO_4	0.2–0.5 μm	10–1800 ppm
Enstatite	$MgSiO_3$	0.2–0.5 μm	10–1800 ppm
Amorphous silicate	variable	0.2–0.5 μm	20–3600 ppm
D-rich organics	HCNO	n.d.	n.d.
Carrier of P1 (=Q) noble gases	Probably organic compounds	n.d.	n.d.

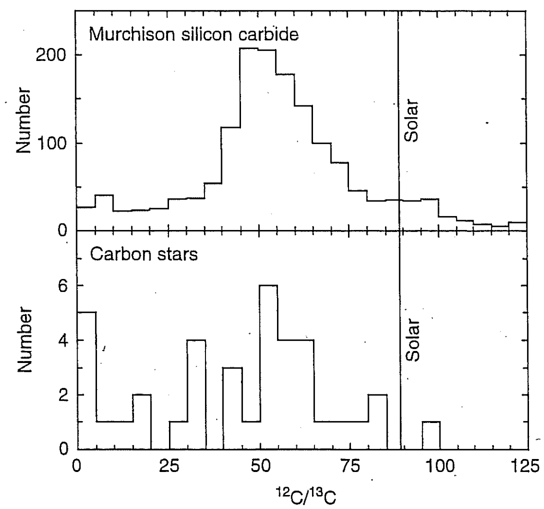

Fig. 5.5 Carbon isotopic compositions of silicon carbide grains from the Murchison meteorite compared with the carbon isotopic compositions of carbon stars (low- to intermediate-mass AGB stars). The composition of carbon in the solar system is indicated by the vertical line. Note the similarity in the distributions of compositions in the two plots. These data indicate that the silicon carbide in the Orgueil meteorite came from a population of carbon stars very similar to that in the galaxy today.

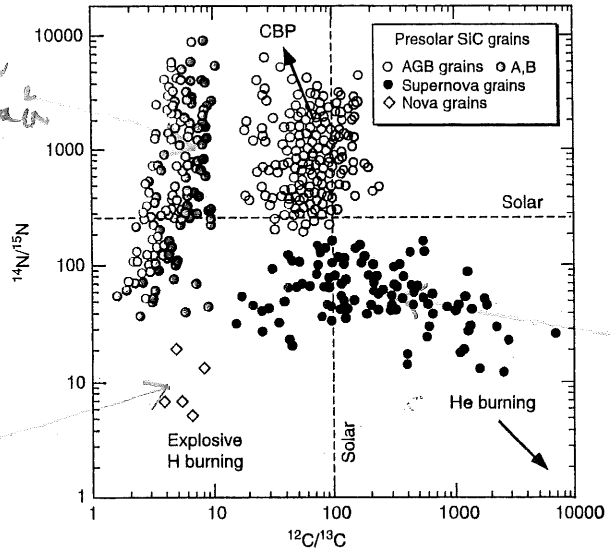

Fig. 5.7 Carbon and nitrogen isotopic ratios for presolar silicon carbide grains. The vast maj(AGB grains) plot above and to the left of the solar composition (indicated by the d Grains with $^{14}N/^{15}N$ ratios >2000 and $^{12}C/^{13}C$ ratios <40 are not predicted by standa But if extra mixing (cool-bottom processing, CBP) is put into the models, compositi the direction of the arrow. Supernova grains, which are rich in ^{12}C from helium burr lower right quadrant. Rare grains thought to come from novae, which are powered hydrogen burning, plot in the lower left quadrant. The sources for the A and B grair currently known, but some may be AGB grains. Modified from Zinner (2004).

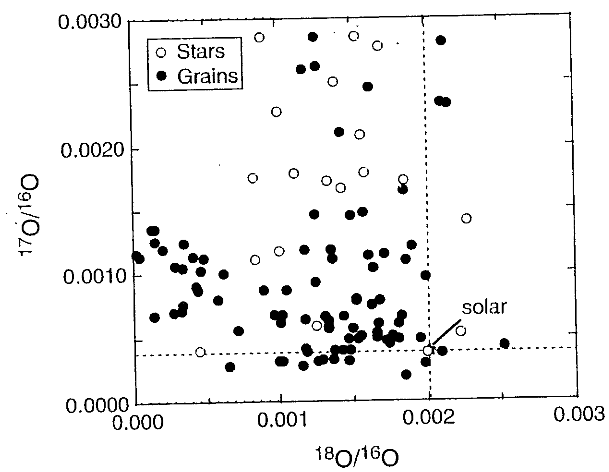

Oxygen isotopic compositions of presolar oxide grains compared with those of red giant sta Stellar data are shown without error bars, which are large on this scale. Both data sets are characterized by higher $^{17}O/^{16}O$ ratios and lower $^{18}O/^{16}O$ ratios compared to solar oxygen. data from Smith and Lambert (1990).

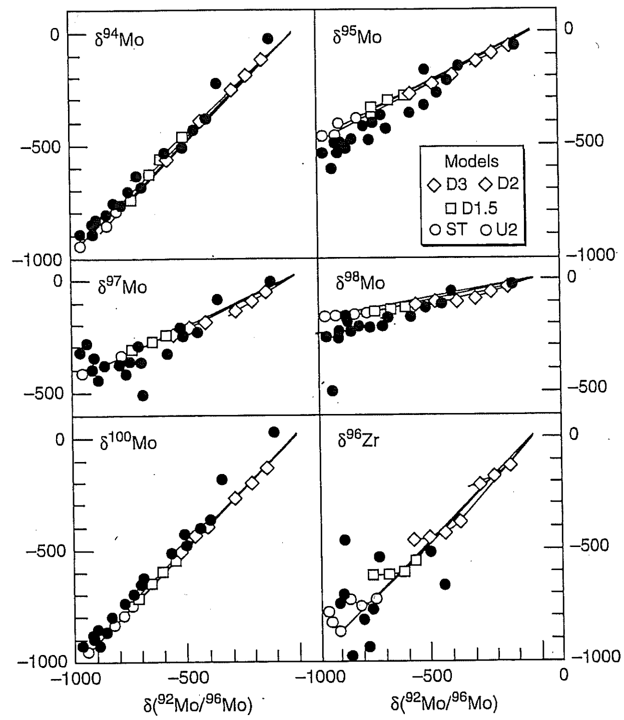

Fig. 5.11 Isotopic compositions of molybdenum in presolar silicon carbide grains compared with model predictions for a 2 $M_\odot$ AGB star with initial solar metallicity. The models shown differ in the strength of the ^{13}C neutron source. The models match the grain compositions well except that the grains tend to lie below the predictions of $\delta^{95}Mo$ vs. $\delta^{92}Mo$, suggesting that the neutron-capture cross-section for ^{95}Mo may need to be re-measured. Data from Nicolussi *et al.* (1998).

Table 9.1 Nuclides used for cosmic-ray exposure ages

Nuclide	Half-life	Produced From
^{3}H	12.26	O, Mg, Si, Fe
^{3}He	stable	O, Mg, Si, Fe
^{10}Be	1.5×10^{6}	O, Mg, Si, Fe
^{14}C	5730	O, Mg, Si, Fe
^{21}Ne	stable	Mg, Al, Si, Fe
^{22}Na	2.6	Mg, Al, Si, Fe
^{26}Al	7.17×10^{5}*	Si, Al, Fe
^{38}Ar	stable	Fe, Ca, K
^{36}Cl	3.01×10^{5}	Fe, Ca, K
^{81}Kr	2.29×10^{5}	Rb, Sr, Y, Zr

*Note that the cosmic-ray community uses a different half-life for ^{26}Al than the one used for early solar system studies.

COMPOSITIONS OF ASTRONOMICAL OBJECTS AND NUCLEOSYNTHESIS

Signatures of nucleosynthesis may be directly observable or convolved with other `astrophysical' factors:
Limiting cases - fresh supernovae ejecta
- run of El/H with (say) Fe/H in the Galactic disk and halo

energy curves

Corollary: we may use accepted ideas of nucleosynthesis with observations of El/H vs Fe/H to infer aspects of the history of a stellar population:
e.g., [O/Fe] vs [Fe/H]

Determination of compositions by spectroscopy calls on atomic and molecular data of many varieties - identification of lines from laboratory spectroscopy, excitation energies, ionization/dissociation energies, oscillator strengths (Einstein A values, gf-values), photoionization/photodissociation cross sections, excitation cross sections (e(H) + A <--> e(H) + A*) etc.

COMPOSITIONS OF ASTRONOMICAL OBJECTS AND NUCLEOSYNTHESIS

Laboratory and in situ analyses

- -- Earth (differentiated) Moon and planets (ditto)
- -- Meteorites
  - carbonaceous chondrites (bulk material)
  - occluded noble gases okay for isotopic ratios (?)
  - presolar grains: C-rich (e.g., SiC, graphite, diamonds) and O-rich (e.g., silicates)
- -- Solar wind - FIP effect but okay for isotopic ratios

Galactic cosmic rays

- -- Living proof of spallation production of LiBeB and other nuclides (Pagel Fig. 9.1)
- -- Abundances at source require correction for alteration of composition in transit from source to detector (spallation)
- -- General identity of source(s) still in dispute
- -- Acceleration mechanisms still under investigation

COMPOSITIONS OF ASTRONOMICAL OBJECTS AND NUCLEOSYNTHESIS

Stellar compositions

Nucleosynthesis occurs internally - out of sight but for emission of neutrinos (solar neutrinos, SN1987A)

Nucleosynthesis in active regions on stellar surfaces has often been invoked in the past and occasionally still but no convincing observational evidence (solar flares?) -- possibly Li and 6Li and 7Li? D?

COMMON ASSUMPTION - For many stars, especially main sequence stars, the atmospheric composition is the initial composition of the star and the composition of the interstellar cloud from which the star formed.

But there are obvious exceptions and some not so obvious exception too where the composition is peculiar and yet very unlikely to be related to nucleosynthesis effects!! For example, chemically B-F peculiar stars - common and poorly understood - where nucleosynthesis is a very unlikely explanation. Also, stars suffering from dust-gas winnowing (Lambda Boo stars, RV Tauri and related stars).

Bringing stellar nucleosynthesis into view

Extensive mass loss (Wolf Rayet stars)
Mixing between interior and surface - convection (Red giants) and rotation (massive main sequence stars)
Mass exchange across a binary system (Ba stars, Algol systems,...)

Ejecta - explosive cases (Supernovae Ia and II), novae
- quiescent cases (Red giants winds/circumstellar shells, planetary nebulae, stellar nebulae)

Table 9.1. *Destruction of light nuclei in stellar interiors*

^{2}D	destroyed by	$(p,\gamma)\,^{3}$He	for $T >$	0.5 ›
^{6}Li	" "	$(p,\alpha)\,^{3}$He	for $T >$	2 ›
^{7}Li	" "	$(p,\alpha)\,^{4}$He	for $T >$	2.5 ›
^{9}Be	" "	$(p,\alpha)\,^{6}$Li; $(p,\,$D$)\,^{8}$Be$\rightarrow 2\,^{4}$He	for $T >$	3.5 ›
^{10}B	" "	$(p,\alpha)\,^{7}$Be$\,(EC)\,^{7}$Li	for $T >$	5.3 ›
^{11}B	" "	$(p,\alpha)\,^{8}$Be$\rightarrow 2\,^{4}$He	for $T >$	5 ›
^{3}He	" "	$(^{3}$He$,\alpha)\,^{4}$He$\,+\,2\,^{1}$H	for $T >$	[illegible]

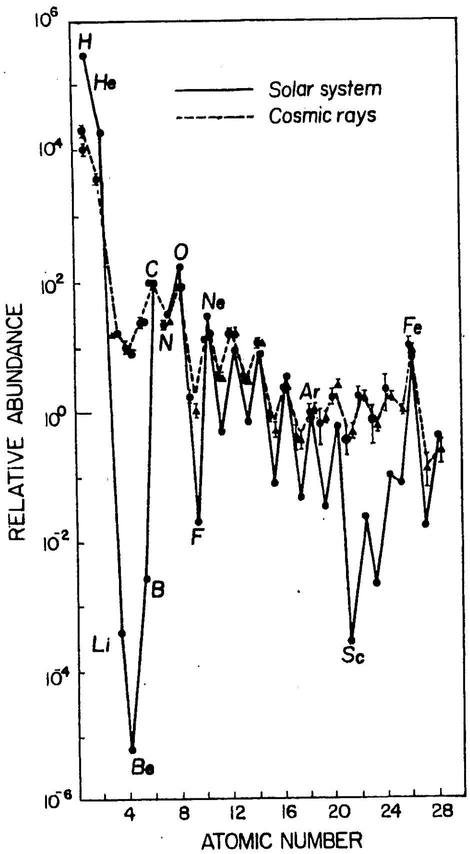

Fig. 9.1. Abundances in primary cosmic rays reaching the top of the Earth's a sphere, compared to Solar-System abundances. (Both normalized to C = After Rolfs and Rodney (1988). Copyright by the University of Chicago. Cou Claus Rolfs.

COMPOSITIONS AND NUCLEOSYNTHESIS

Compositions of astronomical objects

-- tangible objects: count atoms...
  + meteorites
  + Moon, planets, comets ...
  + cosmic rays
  + solar wind
  + interstellar ions

-- intangible objects: spectroscopy --> composition
  + stars, H II regions, H I regions (cool and cold gas), galaxies, Lyman alpha clouds, radioactive ejecta

Signatures of nucleosynthesis may be directly observable but often convolved with (too many?) other `astrophysical' factors.

Pure or almost pure signatures: examples=
  + Tc in AGB stars
  + Wolf-Rayet stars
  + fresh supernovae ejecta
  + fresh novae - see recent discovery of Be-7 and Li-7 enrichments

Convolved signatures: examples=
  + Run of [El/H] vs [Fe/H] within a stellar population, as in the Galactic thin disk, thick disk and halo:
    e.g., [O/Fe] vs [Fe/H] revealing history of SN II and SN Ia contributions;
      abundance variations within a given globular cluster revealing contributions of multiple stellar populations;

Special case of Galactic Cosmic Rays:
  + Observations clearly show that GCRs synthesize LiBeB but to determine the composition of the GCR SOURCE must calculate nuclear evolution of composition from source to us.

COMPOSITIONS AND NUCLEOSYNTHESIS

Determinations of compositions of `tangible' and `intangible' objects with the aim of extracting evidence of nucleosynthesis depend in general on the precision of the analytical tools. Advances in the tools and, particularly, applications of new tools, often, even inevitably, result in new opportunities and new challenges to our understanding.

Discovery of interstellar grains in meteorites came from clever chemical techniques enabling isolation of these small and rare grains within the bulk meteorite in parallel with refined techniques for measuring accurately a variety of isotopic ratios for the separated grains.

For intangible objects,

Advances in the acquisition of spectra are often key to new information: new spectral windows (e.g., IGRINS), higher spectral resolution and higher S/N ratio;

Advances in atomic and molecular physics always applicable: Einstein A-values or gf-values, photodissociation energies, classification of spectra, and plethora of data needed for accurate Non-LTE calculations, ..., and data needed to establish an adequate model of the object, ...